STM JOURNALS

Journal of
Polymer & Composites

ISSN: 2321-2810 (Online)
ISSN: 2321-8525 (Print)
Volume 13, Special Issue 6, 2025
DOI (Journal): 10.37591/JoPC

https://journals.stmjournals.com/jopc

Research JoPC

Effect of Welding Factors on Nugget Size of Polymer-Metal Composite Sheets Using Computational Methods

Amruta Mayur Pasarkar[1], Shankar Kadam[2], Nand Jee Kanu[3,*], Nilesh Raut[4], Pramod Rahate[5], Avinash Datarkar[6]

Abstract

Resistance spot welding (RSW) is a vital technique for joining materials in industries like automotive and aerospace. This study extends the application of RSW to polymer-metal composite sheets by developing 2D axisymmetric, thermo-electro-mechanical coupled model in ANSYS. The focus is on analyzing the temperature distribution, nugget formation, and parameter optimization in hybrid composite sheets, emphasizing the unique challenges posed by polymers' thermal and electrical properties. These properties differ significantly from metals, making it difficult to directly apply existing RSW models developed for metallic sheets. Nimonic 90 sheets, chosen for their high strength-to-weight ratio and excellent thermal properties, were used as a benchmark to provide both industrial relevance and a reliable thermal comparison. This validation focused on temperature distribution and nugget size at the sheet contact surface, demonstrating close agreement with published data. This work provides insights into the integration of composite materials in welding applications, optimizing joint quality and process efficiency. Including Nimonic 90 allows the study to showcase the versatility of the 2D axisymmetric thermo-electro-mechanical coupled model. The model consists of convective heat loss at the electrode/air and workpiece/air interfaces, considering atmospheric 21 °C still air and a coefficient of convection around 15 W/m^2 ˚C. Using a coefficient of convection around 300 W/m^2 ˚C, cooling water at a temperature of 10 ˚C is delivered to the water/electrode interface. The mechanical load of 3000 N is given to the surface of the upper electrode. The model is based on 2D axisymmetric assumptions, with isotropic material properties and simplified boundary conditions to maintain computational efficiency. While earlier studies mainly focused on metallic materials, limited work has addressed polymer-metal composites. This study extends existing RSW models to hybrid systems, underlining its novelty. By examining its behavior, the research can bridge the gap between traditional metallic alloys and hybrid polymer-metal composites.

Keywords: Resistance Spot Welding (RSW), Polymer-Metal Composites, Axisymmetric Modeling, Thermo-Electro-Mechanical Coupling, Nugget Formation

***Author for Correspondence**
Nand Jee Kanu
[1,2,4,6]Assistant Professor, Department of Mechanical Engineering, Bharati Vidyapeeth's College of Engineering, Lavale, Pune, Maharashtra, India
[3]Assistant Professor, Department of Mechanical Engineering, JSPM Narhe Technical Campus, Pune, Maharashtra, India
[5]Associate Professor, Department of Mechanical Engineering, Bharati Vidyapeeth's College of Engineering, Lavale, Pune, Maharashtra, India

Received Date: July 25, 2025
Accepted Date: September 20, 2025
Published Date: October 10, 2025

Citation: Amruta Mayur Pasarkar, Shankar Kadam, Nand Jee Kanu, Nilesh Raut, Pramod Rahate, Avinash Datarkar. Effect of Welding Factors on Nugget Size of Polymer-Metal Composite Sheets Using Computational Methods. Journal of Polymer & Composites. 2025; 13(Special Issue 6): S612–S623p.

INTRODUCTION

Resistance spot welding (RSW) [1] is a versatile technique widely employed in automotive [2, 3] and aerospace industries [4, 5] for joining materials due to its simplicity, efficiency, and ease of automation [6]. This method integrates thermal [7, 8], mechanical [9, 10] and electrical processes [11, 12], making it suitable for diverse material combinations [13, 14]. RSW applies high alternating current (AC) through electrodes under pressure, generating heat via Joule heating at the contact surfaces [15], resulting in molten weld nuggets.

The size and quality of weld nuggets, crucial indicators of joint integrity, depend on parameters

[16, 17] such as welding current, duration, electrode force, sheet thickness, and contact resistance. While traditional applications of RSW focus on metallic materials [18–20], the incorporation of polymer-metal composite sheets [21] introduces unique challenges due to polymers' distinct thermal and electrical properties [22–24]. Numerical simulations [25–27] are essential for addressing these challenges [28, 29], providing insights [27, 30–32] into nugget formation and temperature distribution during welding.

In this study, a 2D axisymmetric, mechanical-electrical-thermal coupled model is developed in ANSYS® [33] to simulate the RSW process for polymer-metal composite sheets. By benchmarking with Nimonic 90 sheets and validating against experimental data for mild steel, the model examines how welding parameters affect temperature variations and nugget formation. This approach extends the application of RSW to advanced hybrid materials [34–37], demonstrating the method's potential in industries [38] prioritizing lightweight and durable structures [39].

Previous studies offer a foundation for understanding critical parameters in RSW. For example, Eisazadeh (2010) [40] analyzed the effects of welding current, electrode pressure, and sheet thickness on nugget formation, while Saleem et al. (2012) [41] highlighted issues like material expulsion due to excessive current. Thakur et al. (2010) [42] explored the interplay of temperature and electrode force, revealing complex stress and strain dynamics [43]. Building on these insights, the current research addresses the unique requirements of polymer-metal composites [28, 44], optimizing joint quality through simulation and parameter analysis. Its inclusion provides a thermal baseline and reflects real industrial applications in aerospace and automotive sectors, strengthening the comparative framework. Its study provides insights into integrating high-temperature alloys with polymers in lightweight structures.

Computational model

A 2D axisymmetric model was developed using ANSYS 14.5 to simulate the resistance spot welding (RSW) process for polymer-metal composite sheets. This modeling approach leverages axisymmetry about the y-axis, enabling an efficient representation of the entire system. The schematic diagram of the 2D model is illustrated in Figure 1.

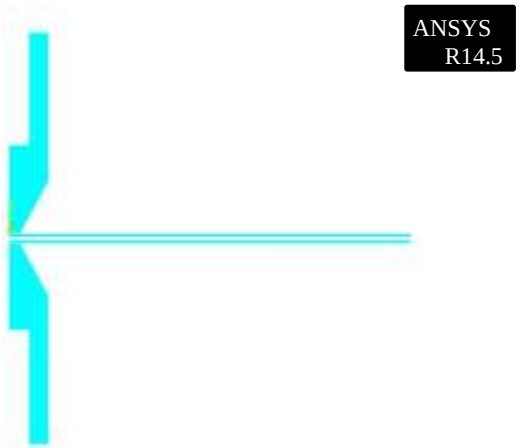

Figure 1. Computational model of RSW.

The model mesh consists of three element types: Plane 223, Contact 178, and Contact 172. These elements represent the thermal, electrical, and mechanical behaviors critical to the RSW process. Plane-223, a solid element, was employed to simulate the coupling effects of thermal, mechanical, and electrical interactions during welding. The contact regions were defined using Contact 178 and Contact 172, representing the interfaces between the electrode and workpiece as well as between workpieces. Three contact surfaces were modeled: two electrode-workpiece interfaces and one workpiece-workpiece interface. These interfaces were assumed to allow slight sliding under the premise of deformable surface contact. Investigating Nimonic 90 in this study creates a baseline for

exploring other hybrid systems. The findings can help develop strategies for welding high-performance alloys with polymer layers in future multi-material designs. By analyzing Nimonic 90's response to welding parameters, researchers can better understand how to adapt these parameters for hybrid polymer-metal composites, ensuring optimal nugget size and weld quality.

Material properties

In RSW, materials undergo extreme temperature variations, making their properties temperature-dependent [43] and non-linear. The thermal and mechanical properties incorporated into the model include thermal conductivity [32], specific heat capacity, and modulus of elasticity, density, and electrical resistivity. These properties are crucial for accurately predicting nugget formation and temperature distribution [45] during welding.

The material properties for steel sheets were adopted from the work of Hou Zhigang et al. (2006) [43], while the data for Nimonic 90 sheets were sourced from the Special Metals Corporation, Huntington, West Virginia. Table 1 summarizes the temperature-dependent material parameters used in the study.

Table 1. Temperature-Dependent Material Properties for Nimonic 90 [46].

Material Properties	**Temperature (˚C)**								
	20	100	200	300	400	500	600	700	800
Thermal conductivity W/m (°C)	11.47	12.77	14.44	15.99	17.54	18.97	20.64	22.32	23.99
Resistivity Ωm (10^{-3})	1.09	1.025	1.042	1.068	1.085	1.110	1.110	1.110	1.110
Specific Heat (J/Kg °C)	446	467	494	520	547	572	600	626	652

The incorporation of temperature-dependent properties ensures the computational model accurately reflects the thermal and mechanical behavior of materials during the welding process. These parameters were instrumental in evaluating the effect of welding parameters on the nugget size and temperature distribution in hybrid composite sheets. The ability to model Nimonic 90's behavior under extreme conditions demonstrates the robustness of the computational framework. This robustness is essential when transitioning to materials with more complex properties, such as polymer-metal composites.

Boundary conditions and loads

A 50 Hz sine wave electrical current flow is applied uniformly to the top surface of the upper electrode, and it is then allowed to travel via the contact surfaces at the electrode-workpiece and workpiece-workpiece interfaces until it reaches the bottom surface of the electrode. Welding current's root-mean-square (RMS) value is represented by Equation (1).

$$I_{rms} = \iint_0^{\pi} 1\,(I_m 2\pi f t)^2 = \frac{I_m}{\sqrt{2}} \tag{1}$$

This value of I_{rms} could be used as DC instead of AC, where I_m is the peak value of welding current and f is the working frequency. The thermal results are not severely affected by the simplification. The lower electrode's bottom face had a zero voltage potential setting. According to Hessamoddin Moshayedi et al. (2012) [47], convective heat loss occurs at the electrode/air and workpiece/air interfaces, considering atmospheric 21 °C still air and a coefficient of convection around 15 W/m^2 ˚C. Using a coefficient of convection around 300 W/m^2 ˚C, cooling water at a temperature of 10 ˚C is delivered to the water/electrode interface. The mechanical load of 3000 N was given to the surface of the upper electrode. Figure 2 shows the boundary conditions applied to the model. The welding factors as considered by Hou Zhigang et al. (2006) [43] are used in this study. Table 2 shows the welding factors. As the current drops, the electrode melts off at a slower rate. The length of the welding arc and the width and volume of the arc cone are both governed by voltage. As the voltage increases, the arc length lengthens (and the arc cone expands), while as the voltage decreases, the arc length shortens (and the arc cone narrows).

Table 2. Applied boundary conditions.

Applied Condition	Value
Frequency	50 Hz
AC Welding current	12.2 kA
Squeeze period	5 cycles (0.1 s)
Time of weld	13 cycles (0.260 second)
Hold period	3 cycles (0.06 s)
Electrode Force	3000 N

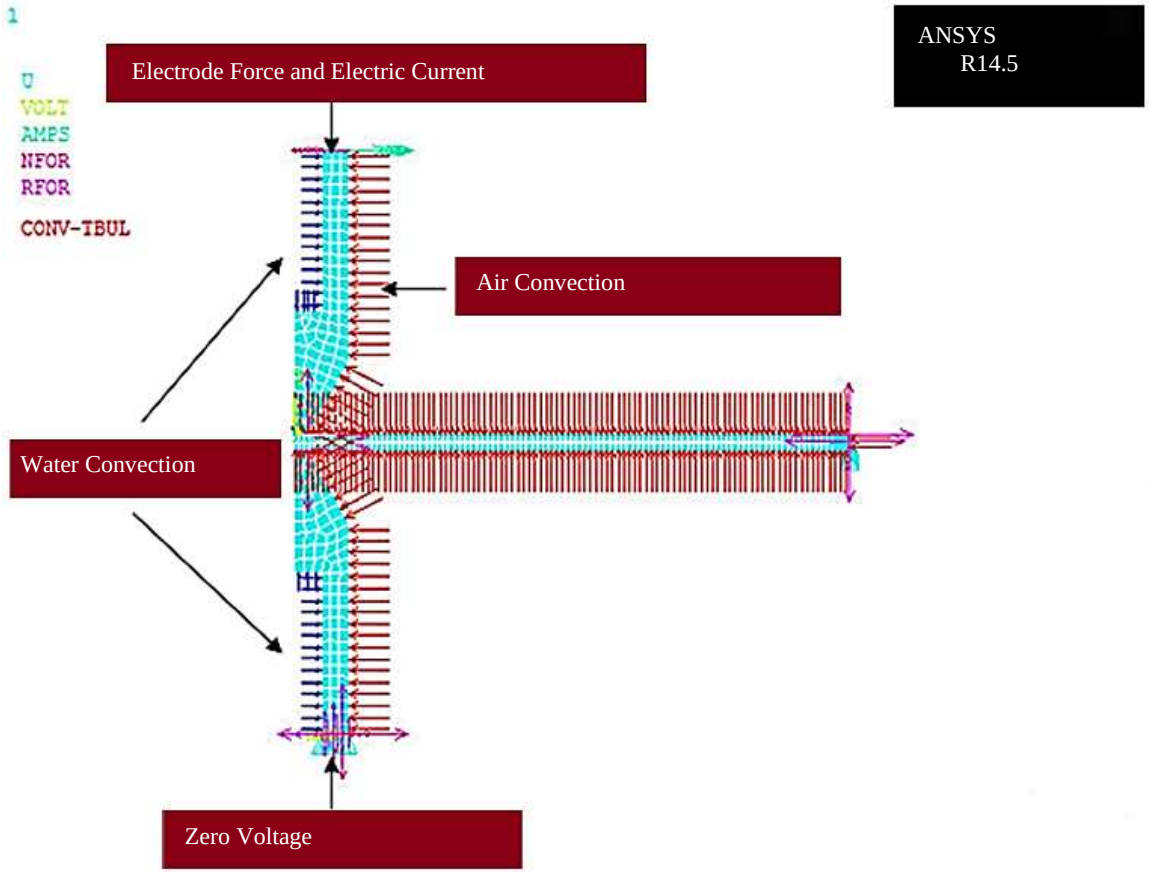

Figure 2. Boundary conditions and loads.

RESULTS AND DISCUSSION

The grid independence test is a process used to determine the optimal grid condition that has the fewest grids while generating the same numerical results. It is based on the evaluation of several grid conditions. The normal welding cycle time is between one and two seconds, with an actual welding duration of a few tenths of a second. The finite element method [9, 25] is used in structural welding modeling to determine the overall and local effects of heat input to a welding assembly. The proportion of a 10-minute period that the welding power supply can continuously output the rated current is known as the welding duty cycle. The thicknesses of Nimonic 90 sheets range from .016 to .156’’. In this work, the RSW process was simulated using a FEM model to examine the phenomenon of nugget formation and the impact of welding parameters on nugget formation and on the temperature variation at the sheet contact surface. The model results were validated against mild steel data, specifically for nugget size and temperature distribution at the sheet contact surface, showing close agreement with published findings. Due to the interaction of the workpiece with temperature and electrode force, the stress field in this process is extremely complex. The application of electrode

force during the squeeze step is what causes the local deformation of the workpiece. A suitable electrical connection is made by the electrode force. As a result, asperities, dust, and surface coatings made of oxide break down. As the asperities are reduced, resulting in lower resistance, the areas that are subjected to greater stress have greater electrical contact.

The temperature rises at the sheet contact surface as the current passes through the electrodes, generating solid state bonding. The stresses are lowest in the middle and largest near the electrode's periphery. Moreover, the edges have more current flow lines than the centre. As a result, the margins have a higher current flow than the centre. When welding first begins, or when the temperature approaches the melting point, heat is created at a greater rate near the edges, and higher stress deformation happens more quickly, resulting in solid state bonding. At the edges, the contact resistances are zero, but at the centre of the sheet's contact surface, the contact resistances are significant and through the centre, the current moves. Then, as depicted in Figure 3, melting begins at the centre point and spreads outward towards the edges.

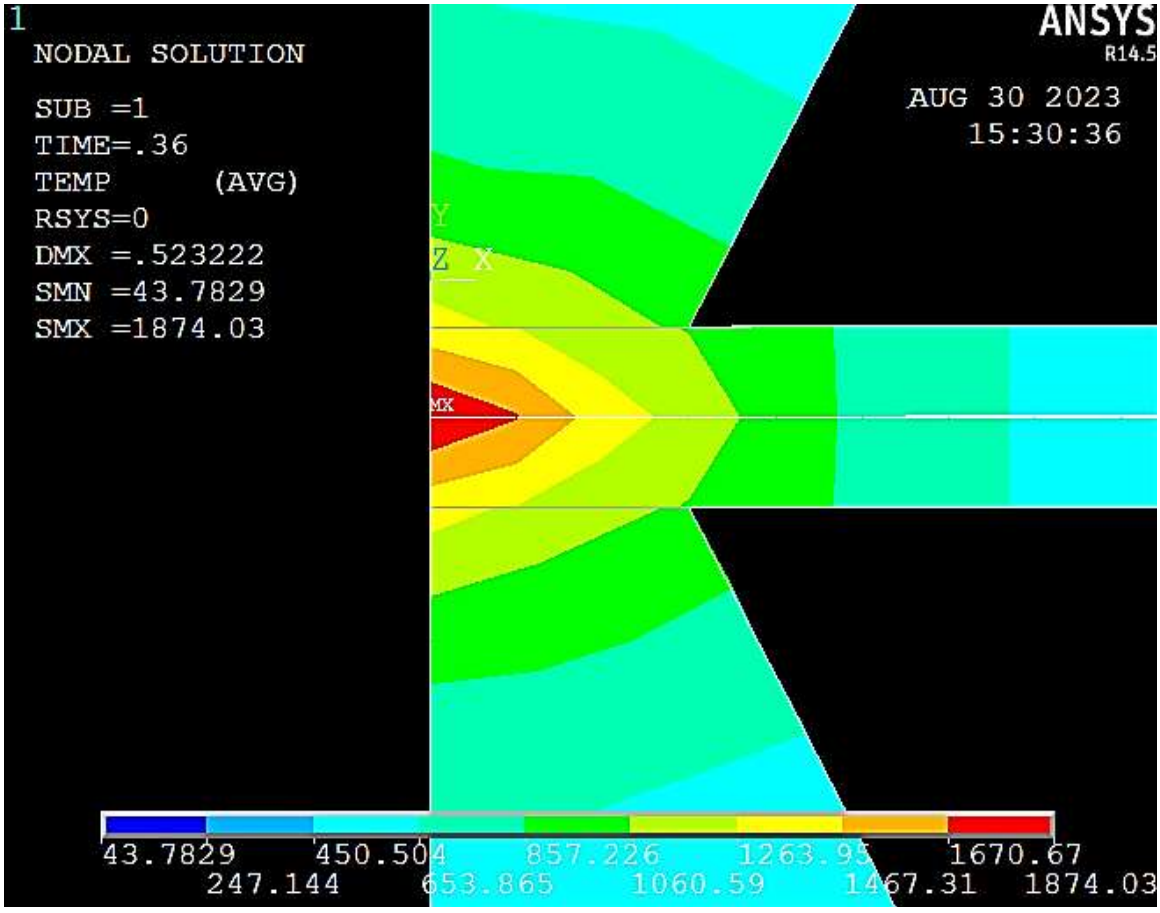

Figure 3. Temperature variation at the conclusion of weld time for mild steel.

The temperature variation at the end of the welding process is shown in Figures 3 and 4. During the start of the welding operation, the temperature at the sheet contact surface rises quickly. The middle of the sheet contact surface has the maximum temperature. Due to the high resistance to the electric current flow at the center of the sheet contact surface, Joule heating occurs at the center and this heat is very high compared to other surfaces. Taking into consideration that the melting point of steel is 1530 ˚C, the nugget is formed at the 10^{th} weld cycle. The weld nugget region is seen red in color. By changing the welding factors, the temperature variation can be changed which changes the nugget size and hence the weld quality. For the hold time, the convection and electrode force are the only external loads acting. The current is removed in this stage. Cooling and solidification of the weldment occurs.

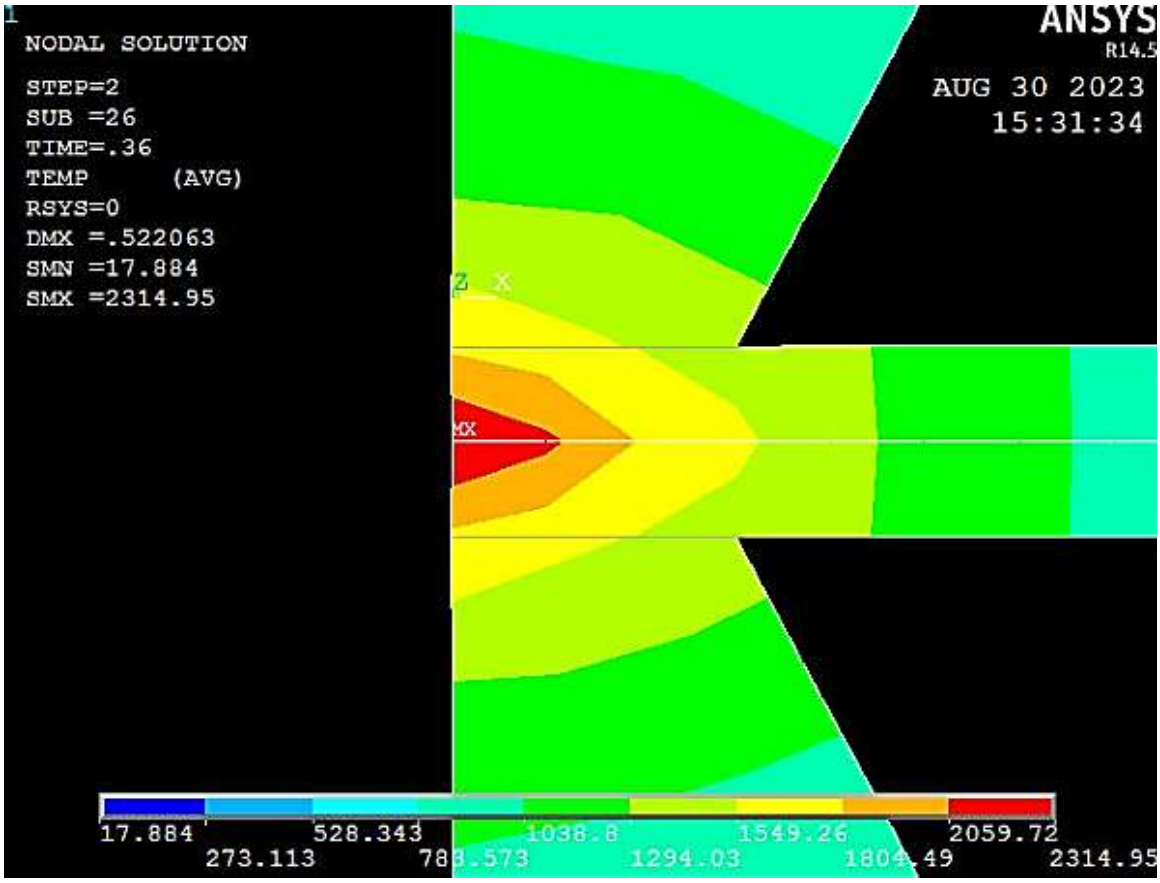

Figure 4. Temperature variation at the conclusion of weld time for Nimonic 90.

The temperature of the nugget decreases instantly. There is a negligible decrease in the size of the weld nuggets compared to that at the conclusion of the weld cycle. Figures 5 and 6 show the temperature variation along the sheet contact surface. In the squeeze stage of RSW process, since only electrode force is applied, heat is not generated and the temperature is very low and remains constant. During the welding stage, the current is passed through the electrodes, thus the Joule heat is generated and temperature at the sheet contact surface rises very rapidly until the current is allowed to flow. The extreme temperature of 1874 ˚C is reached at the completion of the welding cycle for mild steel and 2314.95 ˚C for Nimonic 90.

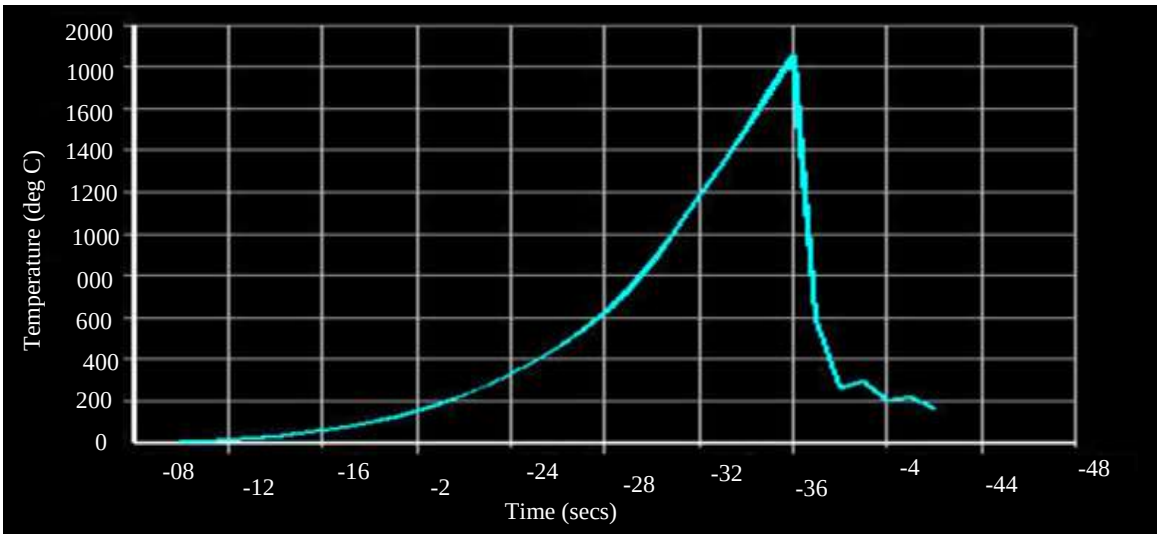

Figure 5. Temperature variation along the sheet contact surface for mild steel.

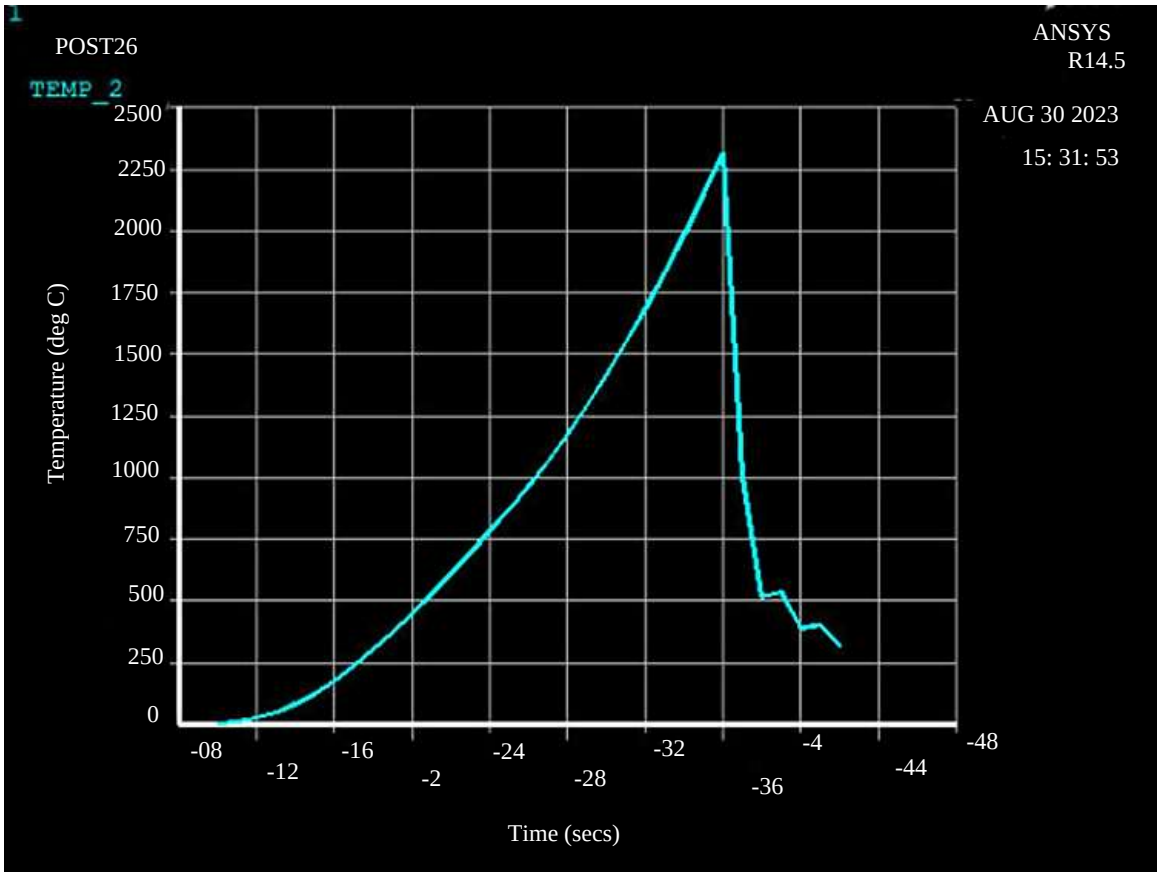

Figure 6. Temperature variation along the sheet contact surface Nimonic 90.

Later, the temperature decreases instantly due to heat loss by convection. Figure 7 depicts the maximum temperature variation with weld time for Nimonic 90. Figure 8 shows the weld size at the starting of the weld cycle as well as at the conclusion of the weld cycle. When the current was allowed to pass through the electrodes, initially the Joule heating at the contact was less, thus the size of the weld nugget was small. The size of the weld rises along with the temperature.

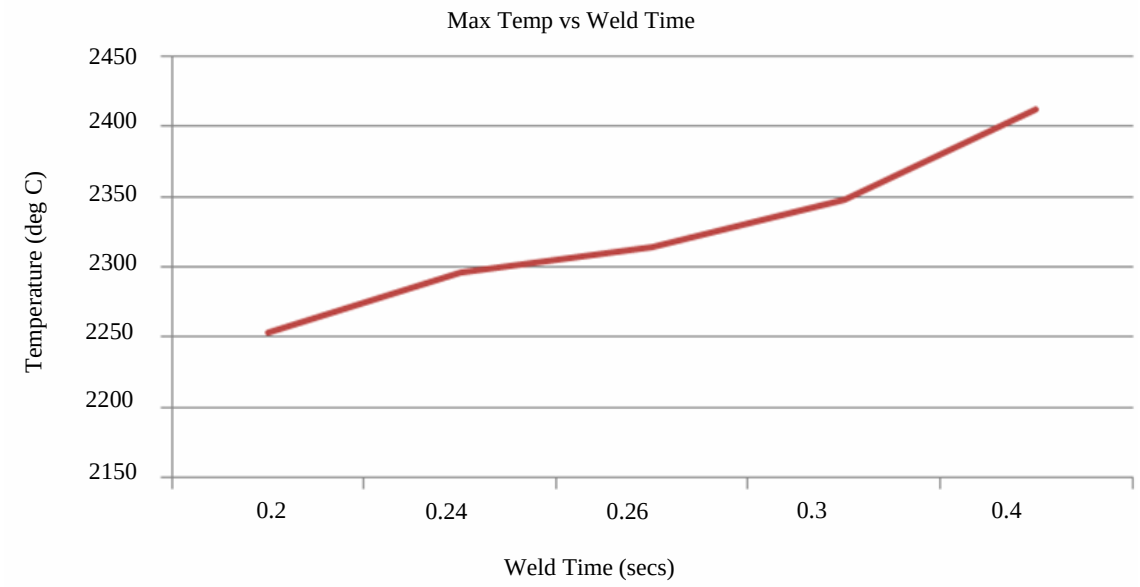

Figure 7. Variation of maximum temperature with weld time for Nimonic 90.

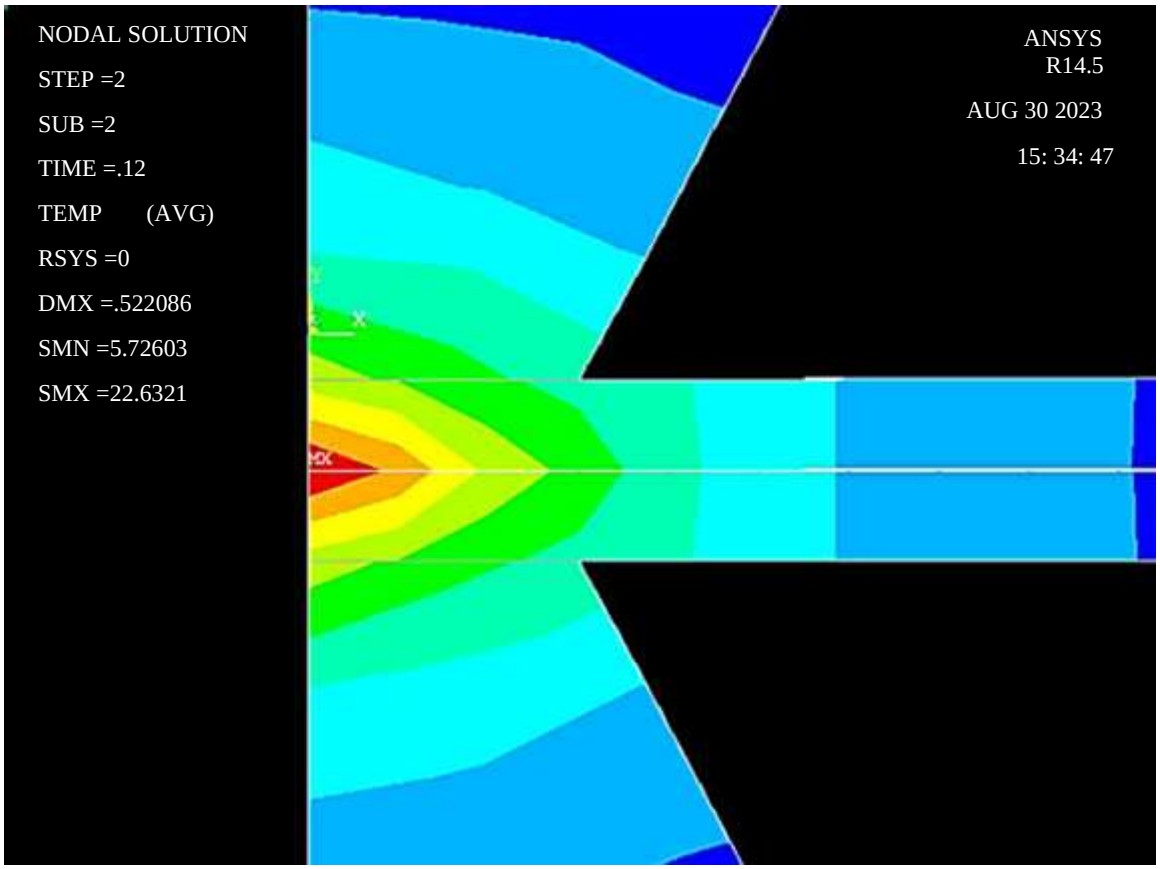

(a)

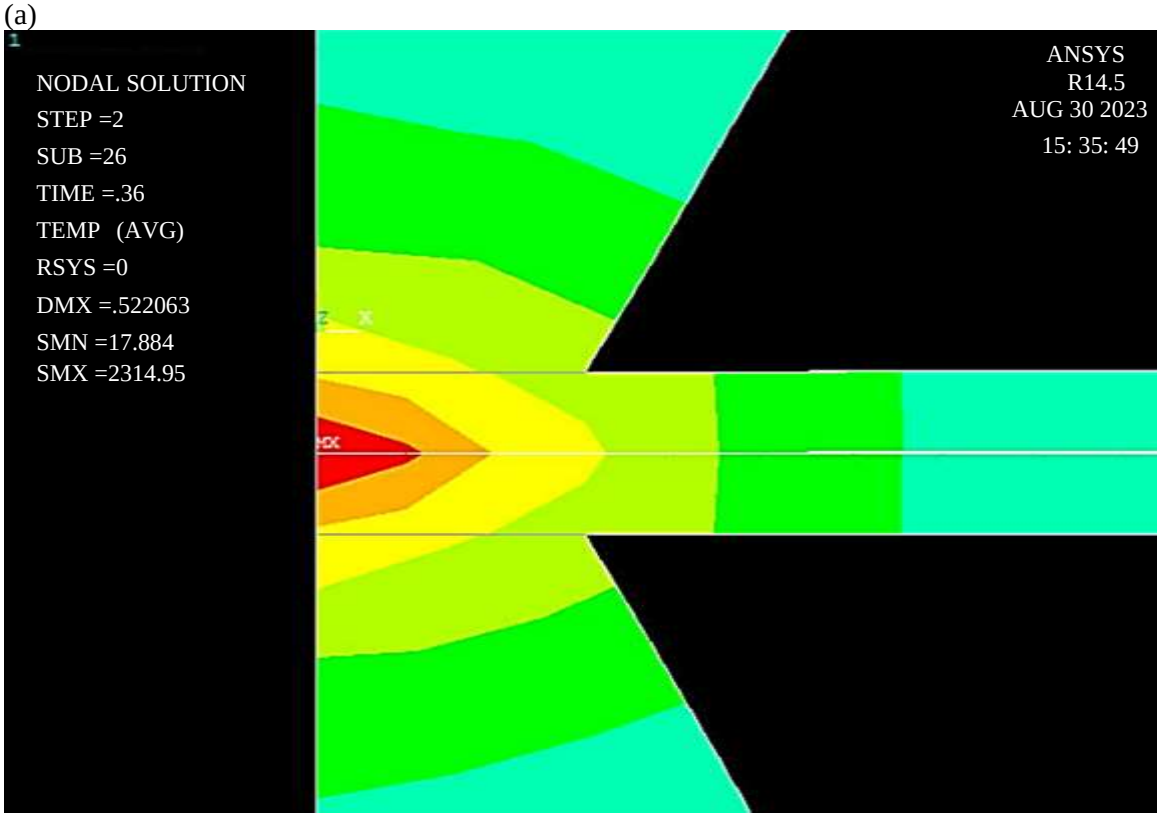

(b)

Figure 8. (a) Weld size when the nugget started to form (b) at the conclusion of the weld cycle for Nimonic 90.

Resistance spot welding produces a molten metal pool that rapidly cools and solidifies into a round joint known as a "nugget" by "welding overlapping pieces of metal at smaller locations by application of pressure and electric current". Spot welding parameters include (a) pressure as in order to produce high-quality welds, the proper amount of pressure or electrode force must be applied, (b) current as the electrical resistance and thermal conductivity of the metal affect how much heat is produced, (c) tip diameter, and (d) the welding cycle. The size of a fillet weld can be determined using the following formula: size of the fillet weld (in.) = 0.707 x thickness of plate (in.).

To produce goods of certain good quality [48], the fundamental requirements for welding quality include the following:

- The bead was unbroken and without holes.
- The bead has waves of uniform height and breadth.
- The final product almost completely lacks distortion and meets the specified dimensions.
- The welded joint has the necessary strength.

Things to consider while choosing the best stick electrode

- Characteristics of base metal
- Tensile strength
- Current for welding
- Thickness, shape, and joint fit-up of the base metal
- Weld positioning
- Specifications and terms of service
- Environmental aspects of the job

Applications such as projection welding inserts, where the electrode contact area is at least three times the weld size, require refractory electrode materials (diameter: >10 mm) like tungsten/copper, tungsten, or molybdenum. The quality of the resistance spot weld is influenced by a number of factors, including electrode geometry, electrode force, welding current and welding time. In addition to the cross-sectional area, the length, ohm rating (i.e., resistance rating), temperature ratings of the insulation material, and ambient temperature also affect the ampacity of the welding cable. In comparison to longer cables of the same diameter, shorter cables can carry more current.

CONCLUSIONS

The investigation introduced a novel approach to resistance spot welding by focusing on polymer-metal composite sheets, extending its application beyond traditional metallic alloys like Nimonic 90. The 2D axisymmetric, coupled thermo-electro-mechanical model accurately simulated the welding process, considering the unique thermal and electrical characteristics of polymer components. The findings underline the potential of RSW in hybrid composites for industries prioritizing lightweight, durable, and efficient materials. The model demonstrated its reliability by aligning with published data for mild steel and successfully predicted the effects of welding parameters on nugget formation and temperature distribution. Future studies can expand this framework to other polymer-composite systems, enhancing joint performance in multi-material structures. Studying Nimonic 90 sheets alongside polymer-metal composites highlights the differences in temperature distribution, nugget formation, and weld quality. This comparative analysis helps refine the model for diverse material combinations.

REFERENCES

1. Vates UK, Sharma BP, Kanu NJ, Daniel NA, Subramanian S, Sharma P. Optimization of Process Parameters of Galvanizing Steel in Resistance Seam Welding Using RSM [Internet]. Vol. 174, Smart Innovation, Systems and Technologies. Springer, Singapore; 2020 [cited 2022 Mar 16]. 695–706 p. Available from: https://link.springer.com/chapter/10.1007/978-981-15-2647-3_65.
2. Kale SM, Kirange PM, Kale T V., Kanu NJ, Gupta E, Chavan SS, et al. Synthesis of ultrathin ZnO, nylon-6,6 and carbon nanofibers using electrospinning method for novel applications. Mater Today Proc. 2021 Jan 1;47:3186–9.

3. Kadam S, Chavan S, Kanu NJ. An insight into advance self-healing composites. Mater Res Express [Internet]. 2021 May 19 [cited 2022 Mar 16];8(5):052001. Available from: https://iopscience.iop.org/article/10.1088/2053-1591/abfba5.
4. Kharadi F, Karthikeyan A, Bhojwani V, Dixit P, Kanu NJ, Jain N. Experimental study of the operating parameters on the performance of a single-stage Stirling cryocooler cooling infrared sensor for space application. Aircr Eng Aerosp Technol. 2023;ahead-of-p(ahead-of-print).
5. Kumsa Gonfa B, Sinha D, Kumar Vates U, Badruddin IA, Hussien M, Kamangar S, et al. Investigation of Mechanical and Tribological Behaviors of Aluminum Based Hybrid Metal Matrix Composite and Multi-Objective Optimization. Materials (Basel) [Internet]. 2022 Aug 16 [cited 2022 Sep 5];15(16):5607. Available from: https://www.mdpi.com/1996-1944/15/16/5607/htm.
6. Kanu NJ, Mangalam A, Gupta E, Vates UK, Singh GK, Sinha DK. Investigation on secondary deformation of ultrafine SiC particles reinforced LM25 metal matrix composites. Mater Today Proc. 2021 Jan 1;47:3054–8.
7. Pandey V, Bekele A, Ahmed GMS, Kanu NJ, Singh GK. An application of conjugate gradient technique for determination of thermal conductivity as an inverse engineering problem. Mater Today Proc. 2021 Jan 1;47:3082–7.
8. Pandey V, Kanu NJ, Singh GK, Gadissa B. AZ31-alloy, H13-die combination heat transfer characteristics by using inverse heat conduction algorithm. Mater Today Proc. 2021 Jan 1;44:4762–6.
9. Kanu NJ, Patwardhan D, Gupta E, Vates UK, Singh GK. Finite element analysis of mechanical response of fracture fixation functionally graded bone plate at paediatric femur bone fracture site under compressive and torsional loadings. Mater Today Proc. 2021 Jan 1;38:2817–23.
10. Vates UK, Khattar N, Kumar R, Bhardwaj A, Sharma BP, Kanu NJ, et al. Al 6063 Hybrid Metal Matrix Reinforced Composites with TiC Nanoparticles and NEEM Leaf Ash Using Stir Casting Method for Bicycle Frame [Internet]. Tyagi RK, Gupta P, Das P, Prakash R, editors. Lecture Notes in Mechanical Engineering. Springer Science and Business Media Deutschland GmbH; 2023 [cited 2023 Nov 14]. 51–65 p. Available from: https://link.springer.com/chapter/10.1007/978-981-99-4758-4_6.
11. Asre CM, Kurkute VK, Kanu NJ. Power generation with the application of vortex wind turbine. Mater Today Proc. 2021 Sep 14;
12. Jain N, Gupta E, Kanu NJ. Plethora of Carbon Nanotubes Applications in Various Fields – A State-of-the-Art-Review. Smart Sci [Internet]. 2021 [cited 2022 Mar 16];10(1):1–24. Available from: https://www.tandfonline.com/doi/abs/10.1080/23080477.2021.1940752.
13. Kanu NJ, Vates UK, Singh GK, Chavan S. Fracture problems, vibration, buckling, and bending analyses of functionally graded materials: A state-of-the-art review including smart FGMS. Part Sci Technol [Internet]. 2019 Jul 4 [cited 2022 Mar 16];37(5):583–608. Available from: https://www.tandfonline.com/doi/abs/10.1080/02726351.2017.1410265.
14. Ayushi, Vates UK, Mishra S, Kanu NJ. Biomimetic 4D printed materials: A state-of-the-art review on concepts, opportunities, and challenges. Mater Today Proc. 2021 Jan 1;47:3313–9.
15. Kumbhalkar MA, Rambhad KS, Kanu NJ. An insight into biomechanical study for replacement of knee joint. Mater Today Proc. 2021 Jan 1;47:2957–65.
16. Vates UK, Kanu NJ, Gupta E, Singh GK, Daniel NA, Sharma BP. Optimization of FDM 3D Printing Process Parameters on ABS based Bone Hammer using RSM Technique. In: IOP Conference Series: Materials Science and Engineering [Internet]. IOP Publishing; 2021 [cited 2022 Mar 16]. p. 012001. Available from: https://iopscience.iop.org/article/10.1088/1757-899X/1206/1/012001.
17. Kanu NJ, Gupta E, Vates UK, Singh GK. Electrospinning process parameters optimization for biofunctional curcumin/gelatin nanofibers. Mater Res Express [Internet]. 2020 Mar 23 [cited 2022 Mar 16];7(3):035022. Available from: https://iopscience.iop.org/article/10.1088/2053-1591/ab7f60.
18. Daniel NA, Vates UK, Sharma BP, Kanu NJ, Subramonian S. Optimization of Inconel Die-In EDD Steel Deep Drawing with Influence of Punch Coating Using RSM [Internet]. Lecture Notes in Mechanical Engineering. Springer, Singapore; 2021 [cited 2022 Mar 16]. 721–738 p. Available from: https://link.springer.com/chapter/10.1007/978-981-33-4320-7_64.
19. Vates UK, Kanu NJ, Gupta E, Singh GK, Sharma BP, Pandey V. Optimization of electro discharge critical process parameters in tungsten carbide drilling using L9 Taguchi approach. Mater Today Proc. 2021 Jan 1;47:3227–34.

20. Chauhan A, Vates UK, Kanu NJ, Gupta E, Singh GK, Sharma BP, et al. Fabrication and characterization of novel nitinol particulate reinforced aluminium alloy metal matrix composites (NiTip/AA6061 MMCs). Mater Today Proc. 2021 Jan 1;38:3027–34.
21. Kanu NJ, Gupta E, Vates UK, Singh GK. An insight into smart self-lubricating composites. Smart Polymer Nanocomposites. Woodhead Publishing; 2021. 85–101 p.
22. Yadav RA, Gautum NK, Dalvi MK, Kanu NJ. Optimizing capacity planning and resource allocation for sustainable supplier development in indian industries. In: AIP Conference Proceedings [Internet]. AIP Publishing; 2025 [cited 2025 May 8]. p. 050004. Available from: /aip/acp/article/3305/1/050004/3345843/Optimizing-capacity-planning-and-resource.
23. Chatur-Deokar M, Halwe-Pandharikar A, Kanu NJ, Yadav RA, Maheshwari A, Deshmukh SJ. Optimizing diesel engine performance and emissions with CuO nanoparticles – Enhanced biodiesel: An RSM approach. In: AIP Conference Proceedings [Internet]. AIP Publishing; 2025 [cited 2025 May 8]. p. 050003. Available from: /aip/acp/article/3305/1/050003/3345757/Optimizing-diesel-engine-performance-and-emissions.
24. Kanu NJ, Kamble AA, Shaikh AN. An insight into energy efficiency for condition based sustainable maintenance. In: AIP Conference Proceedings [Internet]. AIP Publishing; 2025 [cited 2025 May 8]. p. 050006. Available from: /aip/acp/article/3305/1/050006/3345755/An-insight-into-energy-efficiency-for-condition.
25. Kanu NJ, Patwardhan D, Gupta E, Vates UK, Singh GK. Numerical investigations of stress-deformation responses in fractured paediatric bones with prosthetic bone plates. In: IOP Conference Series: Materials Science and Engineering [Internet]. IOP Publishing; 2020 [cited 2022 Mar 16]. p. 012038. Available from: https://iopscience.iop.org/article/10.1088/1757-899X/814/1/012038.
26. Halwe-Pandharikar A, Deshmukh SJ, Kanu NJ. Numerical investigation and experimental analysis of nanoparticles modified unique waste cooking oil biodiesel fueled C. I. Engine using single zone thermodynamic model for sustainable development. AIP Adv [Internet]. 2022 Sep 19 [cited 2022 Sep 20];12(9):095218. Available from: https://aip.scitation.org/doi/abs/10.1063/5.0103308.
27. Gupta E, Kanu NJ, Agrawal MS, Kamble AA, Shaikh AN, Vates UK, et al. An insight into numerical investigation of bioreactor for possible oxygen emission on Mars. Mater Today Proc. 2021 Jan 1;47:4149–54.
28. Kanu NJ, Gupta E, Pendkar SM, Sakhare SA, Munot A, Gupta VK, et al. A Few Suggestions to Improve Anti-drone Measures for Combating Against the Drone Menace. J Inst Eng Ser C 2024 [Internet]. 2024 May 4 [cited 2024 May 9];1–27. Available from: https://link.springer.com/article/10.1007/s40032-024-01047-x.
29. Gupta E, Kanu NJ, Munot A, Sutar V, Vates UK, Singh GK. Stochastic and Deterministic Mathematical Modeling and Simulation to Evaluate the Novel COVID-19 Pandemic Control Measures. Am J Infect Dis [Internet]. 2020 Nov 20 [cited 2022 Mar 16];16(4):135–70. Available from: https://thescipub.com/abstract/ajidsp.2020.135.170.
30. Kanu NJ, Bapat S, Deodhar H, Gupta E, Singh GK, Vates UK, et al. An Insight into Processing and Properties of Smart Carbon Nanotubes Reinforced Nanocomposites. Smart Sci [Internet]. 2022 [cited 2022 Mar 16];10(1):40–55. Available from: https://www.tandfonline.com/doi/abs/10.1080/23080477.2021.1972913.
31. Gupta E, Kanu NJ. An Insight into the Simplified RP Transmission Network, Concise Baseline and SIR Models for Simulating the Transmissibility of the Novel Coronavirus Disease 2019 (COVID-19) Outbreak. Am J Infect Dis [Internet]. 2020 Jul 1 [cited 2022 Mar 16];16(2):89–108. Available from: https://thescipub.com/abstract/ajidsp.2020.89.108.
32. Kanu NJ, Gupta E, Verma GC. An insight into India's Moon mission – Chandrayan-3: The first nation to land on the southernmost polar region of the Moon. Planet Space Sci. 2024 Mar 1;242:105864.
33. Sakhare SA, Pendkar SM, Kanu NJ, Gupta E, Vates UK, Singh GK, et al. Design suggestions on modified self-sustainable space toilet. SN Appl Sci [Internet]. 2022 Jan 1 [cited 2022 Mar 16];4(1):1–23. Available from: https://link.springer.com/article/10.1007/s42452-021-04878-w.
34. Kanu NJ, Lal A. Post buckling responses of carbon nanotubes' fiber reinforced and nanoclay modified polymer matrix hybrid composite plate under in-plane buckling load using the higher order shear deformation theory. Mech Based Des Struct Mach [Internet]. 2022 Oct 5 [cited 2022 Oct 6];1–29. Available from: https://www.tandfonline.com/doi/abs/10.1080/15397734.2022.2126985.

35. Kanu NJ, Lal A. Nonlinear static and dynamic performance of CNT reinforced and nanoclay modified laminated nanocomposite plate. AIP Adv [Internet]. 2022 Feb 1 [cited 2022 Mar 16];12(2):025102. Available from: https://aip.scitation.org/doi/abs/10.1063/5.0074987.
36. Lal A, Kanu NJ. The nonlinear deflection response of CNT/nanoclay reinforced polymer hybrid composite plate under different loading conditions. In: IOP Conference Series: Materials Science and Engineering [Internet]. IOP Publishing; 2020 [cited 2022 Mar 16]. p. 012033. Available from: https://iopscience.iop.org/article/10.1088/1757-899X/814/1/012033
37. Kanu NJ, Lal A. Nonlinear static analysis of CNT/nanoclay particles reinforced polymer matrix composite plate using secant function based shear deformation theory. Smart Sci [Internet]. 2022 Apr 22 [cited 2022 Apr 24];1–12. Available from: https://www.tandfonline.com/doi/abs/10.1080/23080477.2022.2066052.
38. Kanu NJ. Modeling of stress wave propagation in matrix cracked laminates. AIP Adv [Internet]. 2021 Aug 13 [cited 2022 Mar 16];11(8):085217. Available from: https://pubs.aip.org/aip/adv/article/11/8/085217/967766/Modeling-of-stress-wave-propagation-in-matrix.
39. Kanu NJ, Gupta E, Vates UK, Singh GK. Self-healing composites: A state-of-the-art review. Compos Part A Appl Sci Manuf. 2019 Jun 1;121:474–86.
40. Eisazadeh H, Hamedi M, Halvaee A. New parametric study of nugget size in resistance spot welding process using finite element method. Mater Des. 2010 Jan 1;31(1):149–57.
41. Saleem J, Majid A, Bertilsson K, Carlberg T, Nazar Ul Islam M. Nugget formation during resistance spot welding using finite element model. Int Sci Index [Internet]. 2012 [cited 2023 Mar 4];6:707–12. Available from: https://www.researchgate.net/publication/304396448_Nugget_formation_during_resistance_spot_welding_using_finite_element_model.
42. Thakur A., Rasane A, Nandedkar V. Finite Element Analysis of Resistance Spot Welding to study Nugget Formation. Int J Appl Eng Res [Internet]. 2010 [cited 2023 Mar 4];1:483–90. Available from: https://www.researchgate.net/publication/312465609_Finite_Element_Analysis_of_Resistance_Spot_Welding_to_study_Nugget_Formation.
43. Zhigang H, Yuanxun W, Chunzhi L, Chuanyao C. A multi-coupled finite element analysis of resistance spot welding process. Acta Mech Solida Sin. 2006 Mar 1;19(1):86–94.
44. Kanu NJ, Gupta E, Gupta VK. Exploring Black Holes: From Hawking Radiation to Quantum Hair-Insights and Challenges in Modern Astrophysics. J Inst Eng Ser C [Internet]. 2024 Nov 26; Available from: https://link.springer.com/10.1007/s40032-024-01125-0
45. Kanu NJ, Gupta E, Vates UK, Singh GK. An insight into biomimetic 4D printing. RSC Adv [Internet]. 2019 Nov 19 [cited 2022 Mar 16];9(65):38209–26. Available from: https://pubs.rsc.org/en/content/articlehtml/2019/ra/c9ra07342f.
46. Vishwanath MM, Lakshamanaswamy N, Ramesh GK. Numerical Simulation of Heat Transfer Behavior of Dissimilar AA5052-AA6061 Plates in Fiction Stir Welding: An Experimental Validation. Strojnícky časopis - J Mech Eng. 2019 Dec 1;69(4):159–70.
47. Moshayedi H, Sattari-Far I. Numerical and experimental study of nugget size growth in resistance spot welding of austenitic stainless steels. J Mater Process Technol. 2012 Feb 1;212(2):347–54.
48. Patil-Mangore SM, Shegokar NL, Kanu NJ. Conditioning and monitoring of grinding wheels: A state-of-the-art review. J Auton Intell [Internet]. 2023 [cited 2023 Sep 9];6(3):1–23. Available from: https://jai.front-sci.com/index.php/jai/article/view/622/688.

